Supplementary Information for

Thickness-dependent spin Hall magnetoresistance in few-layer $CrPS_4$/Pt heterostructures

Caiqiong Xu[1], Xue He[1], Jicheng Wang[1], Wenxing Chen[1], Shilei Ding[2], Jinbo Yang[3], Yanglong Hou[4,5], Rui Wu[1]**

1. Spin-X Institute, School of Physics and Optoelectronics, State Key Laboratory of Luminescent Materials and Devices, Guangdong-Hong Kong-Macao Joint Laboratory of Optoelectronic and Magnetic Functional Materials, South China University of Technology, Guangzhou 511442, China

2. School of Physical and Mathematical Sciences, Nanyang Technological University, Singapore 637371, Singapore

3. State Key Laboratory for Mesoscopic Physics, School of Physics, Peking University, Beijing 100871, China

4. School of Materials Science and Engineering, Beijing Key Laboratory for Magnetoelectric Materials and Devices, Peking University, Beijing 100871, China

5. *School of Materials, Shenzhen Campus of Sun Yat-Sen University, Shenzhen 518107, China*

* Author to whom correspondence should be addressed: *shilei.ding@ntu.edu.sg*; *ruiwu001@scut.edu.cn*

Contents:

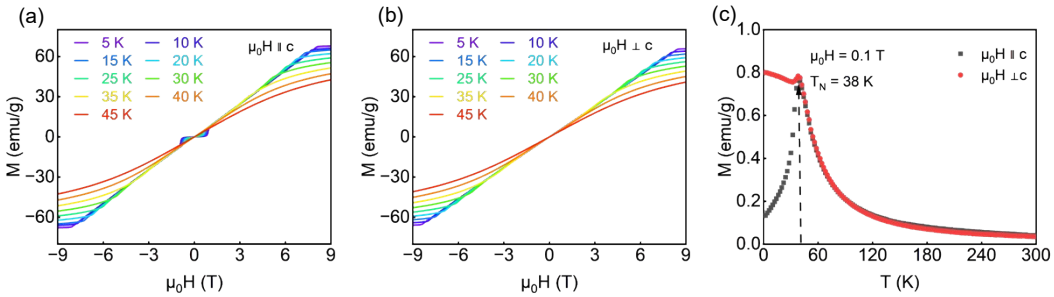

Figure S1. Magnetic characterization of the $CrPS_4$ single crystal. (a) and (b) present the magnetic field dependence of magnetization measured at various temperatures, with the external field applied perpendicular and parallel to the crystalline *c*-axis, respectively. (c) compares the temperature evolution of magnetization under an external magnetic field of 0.1 T applied parallel and perpendicular to the *c*-axis.

Magnetization measurements on bulk single crystals were performed at various temperatures using a vibrating sample magnetometer (VSM) in a Physical Property Measurement System (PPMS, Quantum Design). Figs. S1(a) and S1(b) show the magnetic field dependence of magnetization along the perpendicular ($\mu_0 H \parallel c$) and parallel ($\mu_0 H \perp c$) to the crystalline *c*-axis, respectively, at different temperatures. At 5 K, the magnetization curve for $\mu_0 H \parallel c$ exhibits a typical antiferromagnetic behavior below 0.82 T, characterized by a negligible low-field susceptibility. As the field increases to about 0.82 T, a sharp jump in magnetization occurs, indicating a field-induced spin-flop transition. Beyond this transition, the magnetization increases linearly with the field and finally saturates above 8 T. For $\mu_0 H \perp c$, a linear increase of magnetization with field followed by high-field saturation, is observed, but no magnetic transition is seen in the low-field region. Fig. S1(c) displays the zero-field-cooled magnetization curves measured under $\mu_0 H = 0.1$ T applied parallel and perpendicular to the *c*-axis, from which the Néel temperature of $CrPS_4$ is determined to be 38 K. These observations confirm that the easy axis of $CrPS_4$ lies along the *c*-axis, consistent with previous reports.

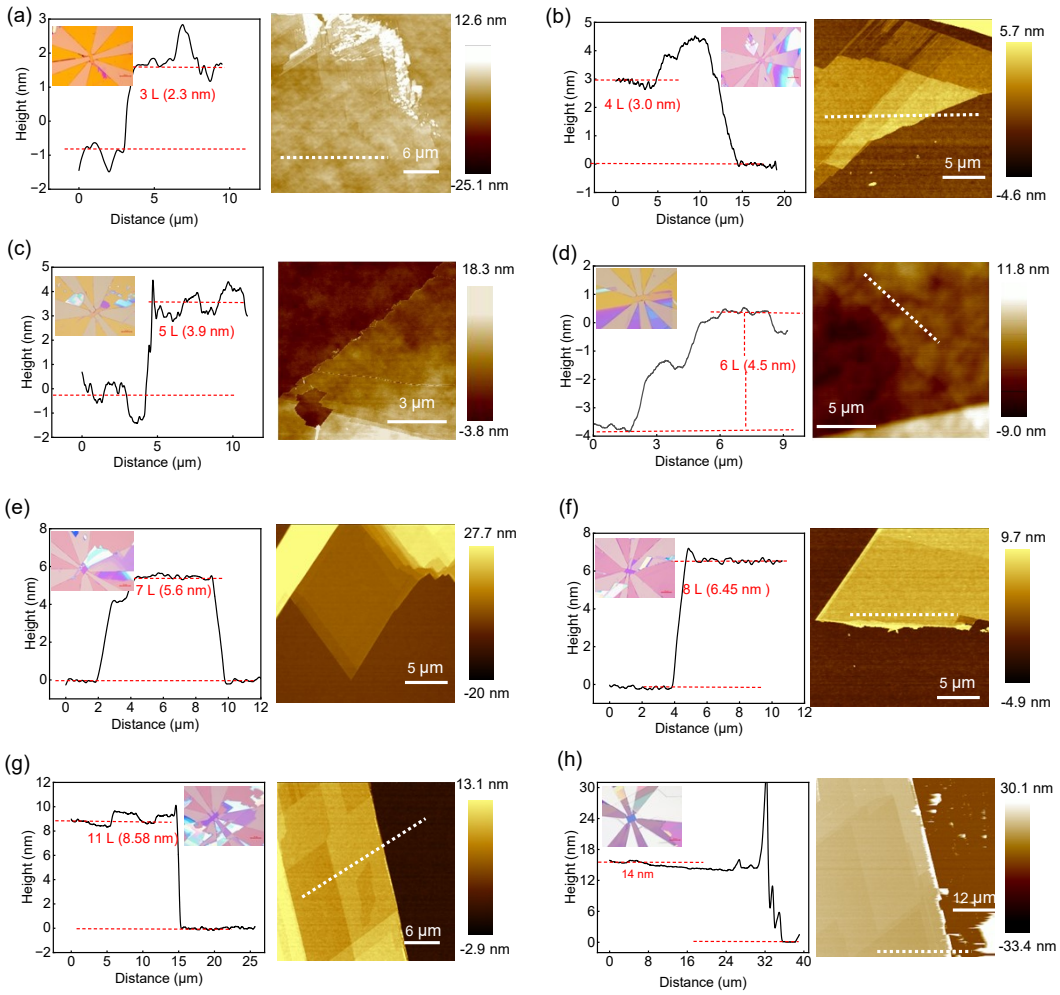

Figure S2. Layer-Dependent Optical Microscopy and Atomic Force Microscopy Images with thickness Data of $CrPS_4$/Pt Devices. (a-h) The thickness of $CrPS_4$ flakes exfoliated on SiO_2/Si substrates characterized using atomic force microscopy (left); $CrPS_4$/Pt devices with different layer numbers fabricated through photolithography and etching (right).

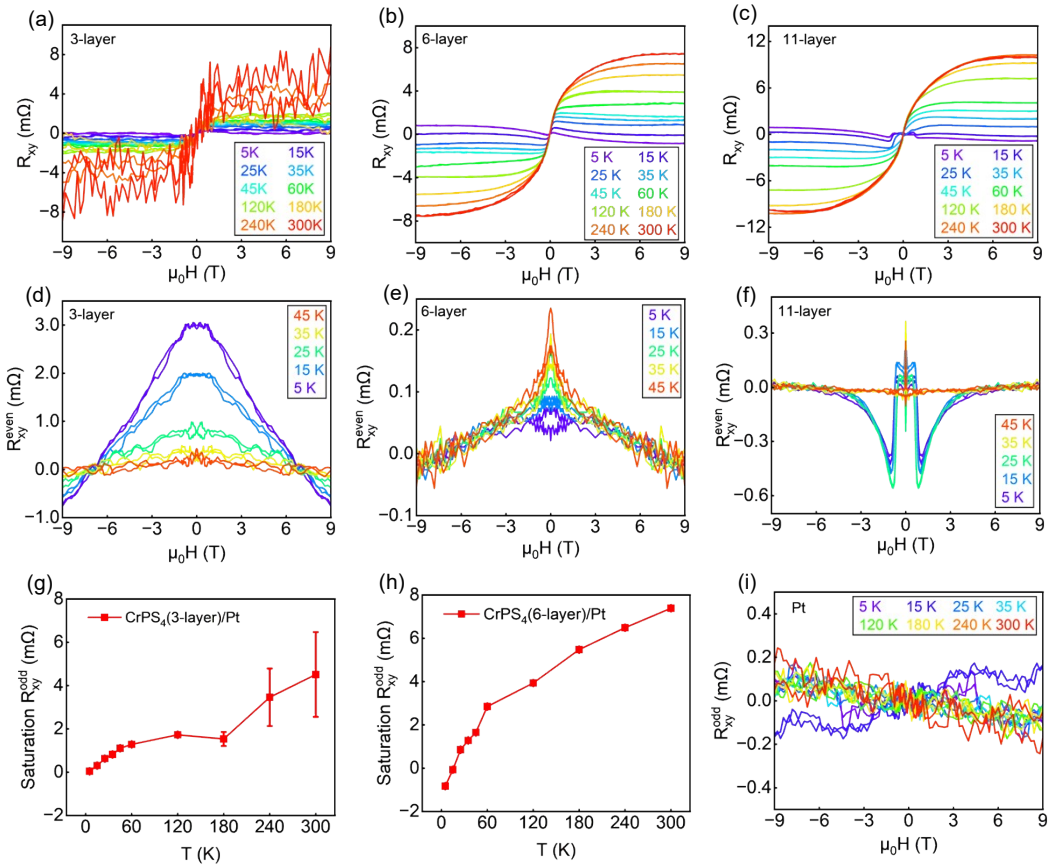

Figure S3. Temperature-dependent anomalous Hall effect in 3-, 6- and 11-layer $CrPS_4$/Pt devices. (a-c) Temperature-dependent R_{xy} signals of the 3-, 6- and 11-layer $CrPS_4$ / Pt device. (d-f) Even components of the R_{xy} signal for 3-, 6-, and 11-layer $CrPS_4$/Pt device at various temperatures. (g, h) The saturation of the R_{xy}^{odd} versus temperature plots for the 3- and 6-layer $CrPS_4$/Pt. (i) Odd components of the R_{xy} signal for Pt device at various temperatures.

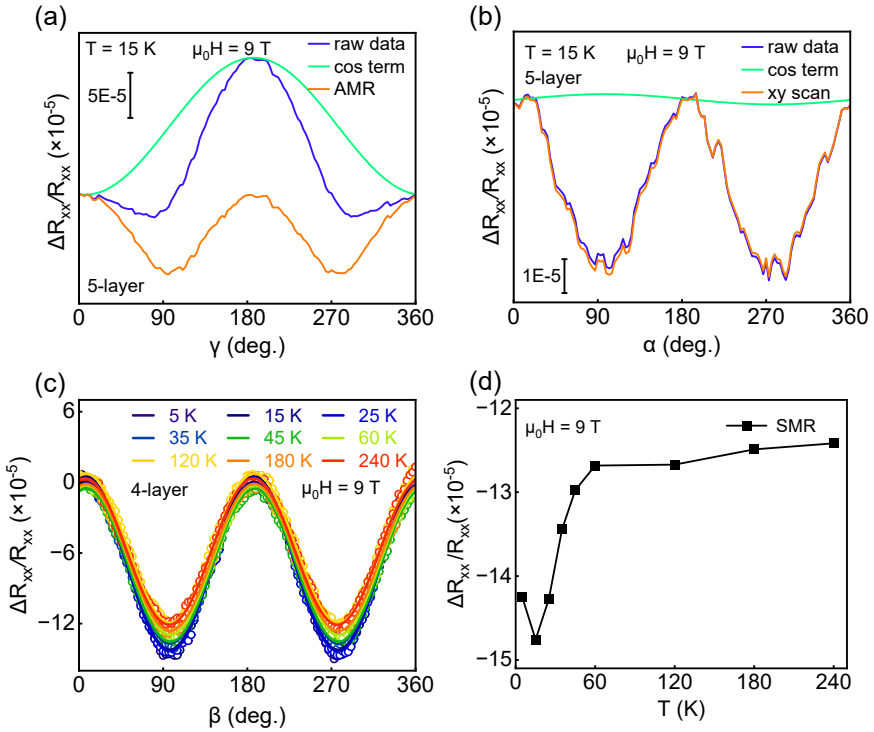

Figure S4. Supplementary data for 4-layer and 5-layer $CrPS_4$/Pt devices. (a-b) The angular dependence of longitudinal resistance upon γ and α, respectively, at various temperatures. Here, the purple curves represent the raw data, the green curves represent the cosine term (which denotes a unidirectional contribution to the longitudinal resistance), and the orange curves in panels (a-b) correspond to the data for the AMR and *xy* scan, respectively. (c) SMR in 4-layer $CrPS_4$/Pt devices of different temperature at 9 T. (d) Temperature evolution of pure SMR in β dependence of longitudinal resistance for 4-layer $CrPS_4$/Pt device at $\mu_0 H = 9$ T

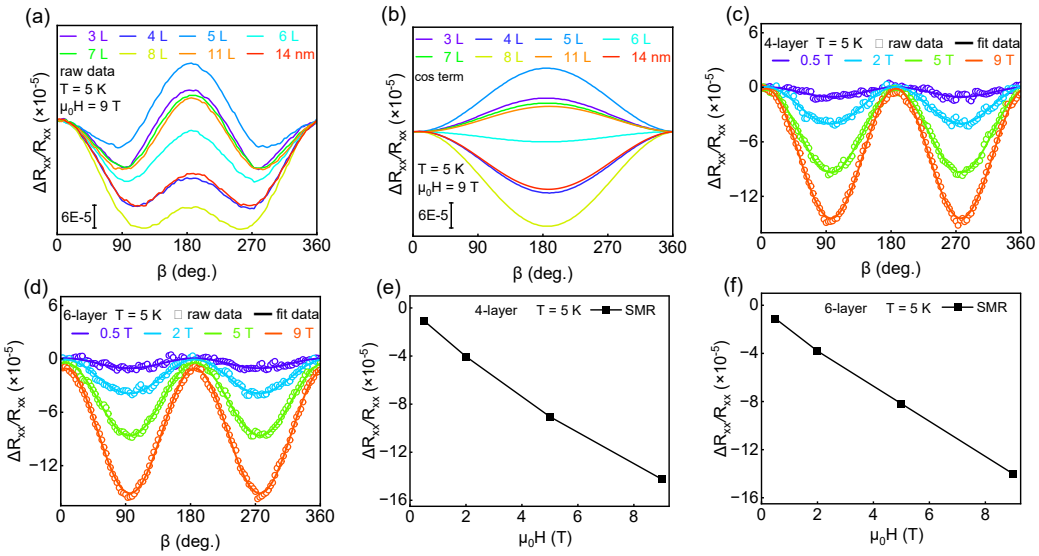

Figure S5. Angular dependence of SMR in few-layer $CrPS_4$/Pt devices under different magnetic fields. (a) Raw data in devices of different thicknesses at 9 T and 5 K. (b) The cosine term in devices of different thicknesses at 9 T and 5 K. (c-d) Angular-dependent SMR under various magnetic fields for 4-, and 6-layer $CrPS_4$/Pt devices at 5 K. (e-f) The magnetic field dependence of the SMR in 4- and 6-layer $CrPS_4$/Pt devices.